ADVANCED INTELLIGENT SYSTEMS
Open Access
www.advintellsyst.com

In Materia Neuron Spiking Plasticity for Sequential Event Processing Based on Dual-Mode Memristor

Linbo Shan, Zongwei Wang, Lin Bao, Shengyu Bao, Yabo Qin, Yaotian Ling, Guandong Bai, John Robertson, Yimao Cai,* and Ru Huang*

Artificial neurons are the fundamental elements in neuromorphic computing systems. Studies have revealed neuronal spike-rate adaptation owing to intrinsic plasticity that neurons will adapt to the spiking patterns and store the events in the background spiking through clustered neuronal spiking. The event can be reactivated by specific retrieval clues instead of solely relying on synaptic plasticity. However, the neural adaptation, as well as the interactive adaptations of neuronal activity for information processing, have not been implemented. Herein, an artificial adaptive neuron via in materia modulation of the VO_2/HfO_2 based dual-mode memristor is demonstrated. By changing the conductance of the HfO_2 layer, the firing threshold can be modulated, thus the excitability and inhibition can be adjusted according to the previous stimuli without any complex peripherals, showing an adaptive firing rate even under the same stimuli. The artificial neuron clusters can emulate the concept of neuronal memory and neural adaptation, demonstrating spatiotemporal encoding capabilities via the correlated neural firing patterns. This conceptual work provides an alternative way to expand the computation power of spiking neural networks by exploiting the neural adaptation and could be enlightenment to maximize the synergy across both synapse and neuron in neuromorphic computing systems.

1. Introduction

In the post-Moore era, computing hardware based on conventional complementary metal–oxide–semiconductor (CMOS) technology is seeking performance enhancement and energy efficiency improvement beyond merely scaling the transistors. New computing paradigms based on emerging devices, such as in-memory computing and neuromorphic computing, are actively explored to break the shackle of the conventional computing architecture. As one of the most promising brain-inspired computing paradigms, the spiking neural networks (SNNs) develops rapidly and has achieved great success in many fields.[1] The neuromorphic chips with SNNs algorithms, such as TrueNorth[2] and Loihi,[3] have shown a significant improvement in performance and energy efficiency in specific tasks. However, these systems are based on CMOS technology, which inevitably induces considerable hardware overhead since dozens of transistors are employed to emulate a single neuron or synapse. The emerging devices, such as resistive random access memory (RRAM),[4–6] phase-change memory (PCM),[7] and insulator–metal transition (IMT) devices,[8,9] are researched to emulate artificial synapses or neurons owing to both area efficiency and performance gain. Meanwhile, great efforts have been made in developing the SNNs algorithms. Spiking coding schemes, including rate coding, temporal coding, spiking correlated coding, and latency phase coding are reported to achieve better performance with less latency, higher efficiency, and smaller hardware overhead.[10,11]

In conventional SNNs, neurons can perform a nonlinear transformation through the integration-and-fire (IF) function, which only employs the basic neuron characteristics. In contrast, the biological neurons show adaptation behaviors that the neuronal activities will decay in response to repeated or prolonged stimulation. The neuron adaptation on a single-cell level

L. Shan, Z. Wang, L. Bao, S. Bao, Y. Qin, Y. Ling, Y. Cai, R. Huang
School of Integrated Circuits
Peking University
Beijing 100871, China
E-mail: caiyimao@pku.edu.cn

The ORCID identification number(s) for the author(s) of this article can be found under https://doi.org/10.1002/aisy.202100264.

DOI: 10.1002/aisy.202100264

Y. Cai, R. Huang
Frontiers science center for nano-optoelectronics
Peking University
Beijing 100871, P. R. China

G. Bai, J. Robertson
Department of Engineering
University of Cambridge
Cambridgeshire CB2 1PZ, UK

Z. Wang
Advanced Institute of Information Technology
Peking University
Hangzhou, Zhejiang 311215, P. R. China

resembles a high-pass filter operation for predictive coding.[12] On a cluster or network level, nonlinear interactions of neuron adaptations are critical in shaping various computing functions including stimulus selectivity, sequence processing, and denoising. Neuron adaptation is widely observed from sensory to motor functional terminals. Researches discover that neuron adaptations can demonstrate context memory properties—that is, the neurons' present response is related to its historical input stimuli, which can enable context memory properties.[13] This adaptation can be attributed to the changes in the neuronal intrinsic plasticity where the firing threshold voltage is adaptive.[14,15] Various forms of intrinsic plasticity can temporarily tune neurons' excitability to achieve powerful information processing abilities. Therefore, emulation of neuron adaptation can further enrich the functionality and empower the computational power of the SNNs-based neuromorphic hardware. Recently, Wang et al. reported a leaky LIF neuron circuit with an adaptive threshold voltage.[16] Although it shows good performance in pattern recognition, the peripheral circuit is very complicated.

In this article, artificial adaptive neurons based on dual-mode VO_2/HfO_2 memristor are designed and experimentally demonstrated. The VO_2 exhibits IMT behavior under voltage stimulation, showing threshold switching characteristics, while HfO_2 is a memristive material with non-volatile memory characteristics.[17,18] Through the synergy of these two characteristics, we realize the in materia modulation of neurons' intrinsic plasticity without additional complex circuits. The IMT threshold voltage can be adaptively changed by tuning the memristive layer, achieving adjustable firing modes even under the same stimuli. Furthermore, we demonstrate that the different input sequences of the same word can be encoded by employing the interaction of multiple adaptive neurons. The results show the proposed adaptive artificial neuron can be implemented to process serial order information through clustered neural adaptation, which enriches the processing capability of neurons to achieve bio-plausible SNNs.

2. Characteristics of VO_2/HfO_2 Device

The dual-mode memristor has a stacked device structure with VO_2 and HfO_2 as the main functional layers. **Figure 1**a shows scanning electron microscope (SEM) images of the 32×32 array (fabrication details are shown in the method section). The cross-point defines the size of a single device ($2\,\mu m \times 2\,\mu m$). The bottom and top electrodes are Pt and TiN, respectively. The Raman spectrum of the as-fabricated VO_2 shows at 190, 223, 260, 309, 389, and 615 cm^{-1}, respectively, indicating the VO_2 is in the M1 phase,[19,20] as shown in Figure 1b,

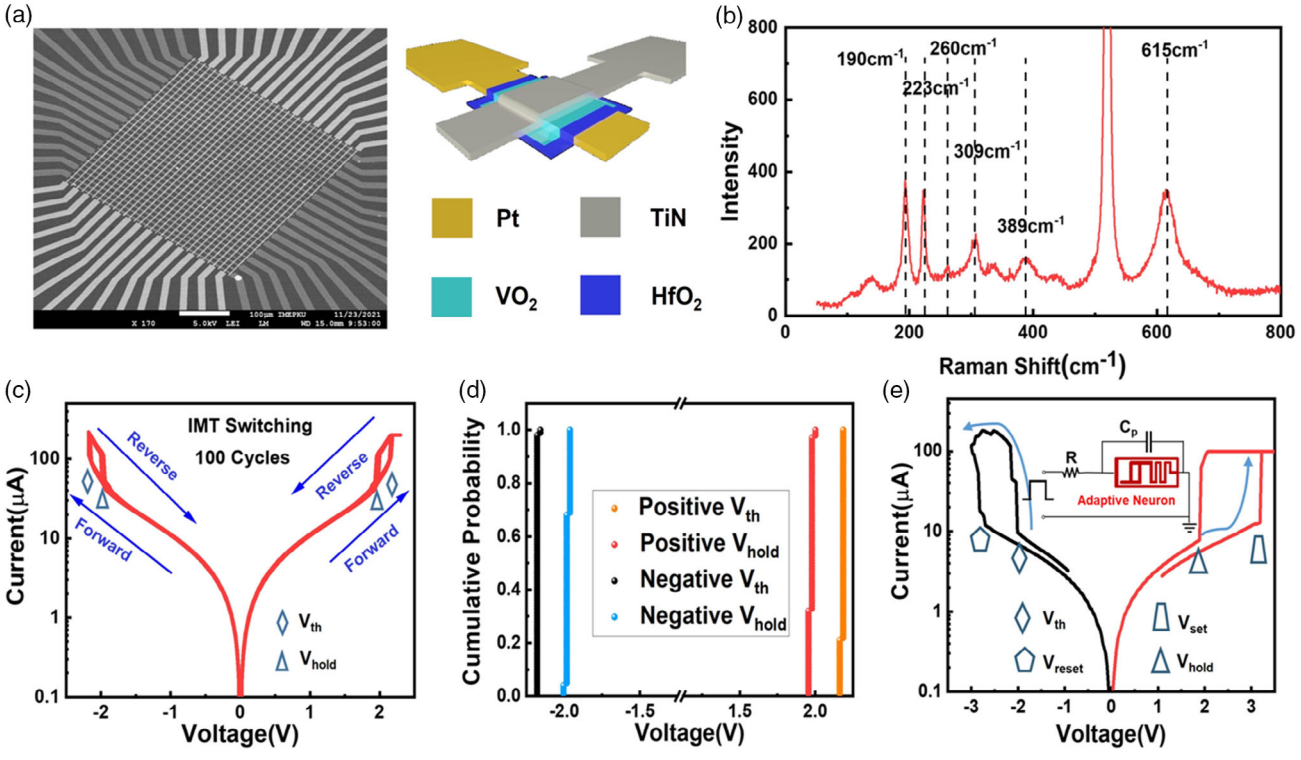

Figure 1. a) Scanning electron microscope (SEM) images of the devices in a 32×32 array. VO_2/HfO_2 is the functional layer. The bottom and top electrode are Pt and TiN, respectively. b) The Raman spectrum of the VO_2 film. The peaks at 190, 223, 260, 309, 389, and 615 cm^{-1} indicate the M1 phase. c) Typical *I–V* curve (100 cycles) when HfO_2 is in NVLRS. d). Distributions of V_{th} and V_{hold}. e) Typical *I–V* curve of the dual-mode memristor. After forming, a negative voltage sweeping is implemented to reset the HfO_2 to HRS (black line). The current abruptly increases at −2.0 V due to the insulator–metal transition (IMT) transition of VO_2. Then, a positive voltage sweeping is implemented to set the HfO_2 to LRS (red line). The current increases at 3.2 V due to the HfO_2 is set to LRS. In the backward sweep, the current suddenly drops at hold voltage (red line). The insert image is the schematic of the measurement configuration.

Supporting Information. The X-ray diffraction (XRD) pattern of the polycrystalline VO_2 is shown in Figure S1, Supporting Information, and indicates the polycrystalline VO_2 mainly consists of the M1 monoclinic phase.[21] The pristine device is in a high-resistance state (HRS), which is mainly determined by the state of HfO_2. A forming voltage (≈5 V) is needed to switch HfO_2 to a low-resistance state (LRS). The states stored in HfO_2 are nonvolatile (NVHRS and NVLRS). Figure 1c shows 100 bidirectional voltage sweeping cycles by repeatedly sweeping from 0 to ±2.2 V. In the forward sweeping, the current will increase abruptly when voltage exceeds the threshold voltage (V_{th}). In the reverse direction, the current abruptly decreases below the hold voltage (V_{hold}). This is consistent with the typical IMT *I–V* curve if the HfO_2 is kept in NVLRS. Figure 1d shows the cumulative distribution of V_{th} and V_{hold} in both positive and negative biases. The tight cycle-to-cycle distribution indicates excellent uniformity. To investigate the device-to-device variation, ten devices are randomly selected and measured for 20 cycles. The statistical results are shown in Figure S2, Supporting Information. By changing the conductance of HfO_2, the V_{th} and V_{hold} can be adaptively adjusted. Figure S3a, Supporting Information, shows gradual reset coupling both IMT and memristive behaviors. The multilevel conductance can be tuned by the reset stop voltage. Figure S3b, Supporting Information, shows the dependence of conductance on reset voltage.

3. Artificial Adaptive Neuron

The adaptation of neurons originates from intrinsic plasticity, which has important applications in the biological neural network.[22,23] Excitation and inhabitation are extreme cases of neuron adaptation. For example, the function of the V0 series neurons in mice is to control their locomotion.[24] V0D neurons and V0V neurons are alternatively activated and inhibited to toggle between "walk slowly" and "trot." This is because the excitability of neurons can be either enhanced or weakened to maintain system stability. Neurons switching between excitation and inhibition state is very important for the nervous system to perform normal physiological functions. Benefiting from the in materia modulation of the memristive layer, the proposed device can easily emulate the excitation and inhabitation of the neuron.

Figure 1e shows the device can be switched between NVHRS and NVLRS with IMT behavior. The test schematic of the oscillatory neuron with adaptation is shown in the inset of Figure 1e. The test circuit includes an external resistor and the intrinsic

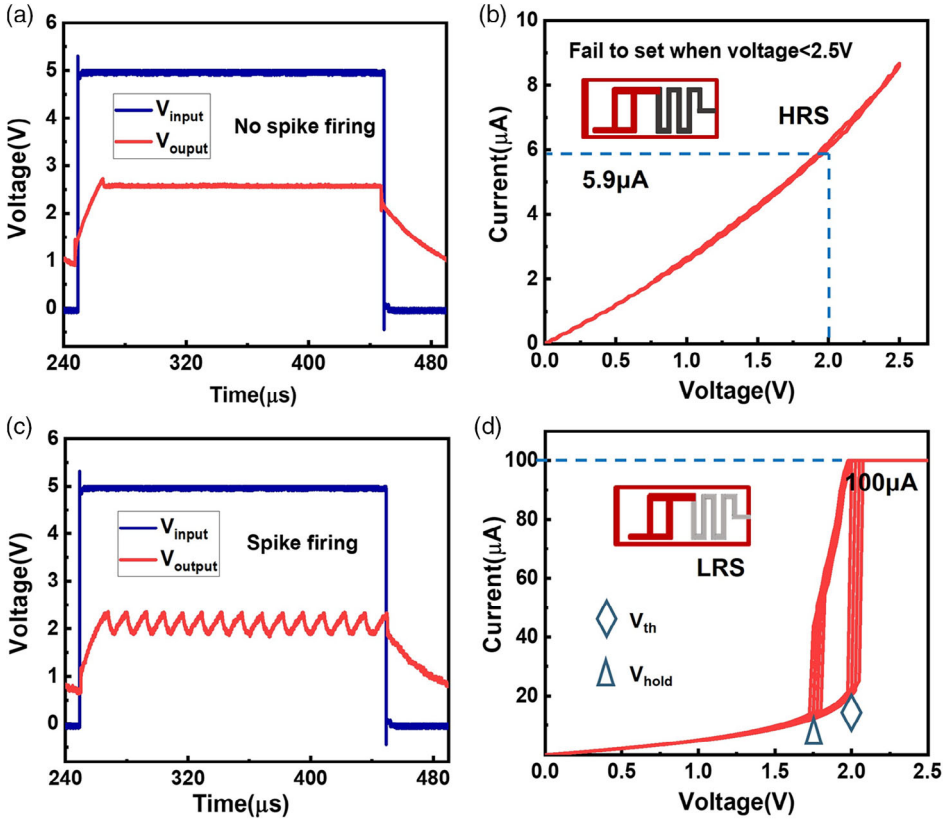

Figure 2. Illustration of excitation and inhibition of the adaptive neuron. a) The input stimulus and measured output waveforms (HfO_2 is in HRS). When 5 V pulse with 200 μs width is applied to the device, the adaptive neuron has no spike firing. b) The *I–V* curve when HfO_2 is in nonvolatile high-resistance state (NVHRS). The current is only 5.9 μA at 2 V. V_{th} of the adaptive neuron exceeds 2.5 V. c) The input stimulus and measured output waveforms (HfO_2 is in nonvolatile low-resistance state (NVLRS)). The adaptive neuron fire spikes when the same stimulus (5 V 200 μs) is applied. d) The *I–V* curve of the device when HfO_2 is in NVLRS. The current reaches the compliance current 100μA at around 2 V.

parasitic capacitance of the device. The value of the load resistor is between the high resistance and low resistance of VO_2. When applying a voltage pulse, most of the voltage drop on the VO_2/HfO_2 device and the parasitic capacitance begin to charge. The charge time is denoted as τ_{rise}. Once the voltage exceeds V_{th}, the VO_2 switches to LRS, which is below the load resistor. At this point, the parasitic capacitance starts to discharge. The discharge time is denoted as τ_{down}. When the voltage decreases below the V_{hold}, the VO_2 returns to HRS. The capacitance will be recharged. As the capacitor charges and discharges repeatedly, the voltage of the VO_2/HfO_2 device oscillates between V_{th} and V_{hold}. The oscillation frequency is determined by τ_{rise} and τ_{down}.

The excitation and inhibition can be controlled by properly configuring the NVLRS and NVHRS, respectively. Figure S3a, Supporting Information, shows a gradual reset property indicating multilevel conductance states. The multilevel conductance can be tuned by the reset stop voltage from −2.5 to −3 V. Figure S3b, Supporting Information, shows the dependence of multilevel conductance on reset voltage. **Figure 2**a shows the inhibition of the artificial neuron. At this time, a 5 V pulse with a 200 µs width is applied to the top electrode. The load resistance is 230 KΩ. Figure 2b indicates the neuron is muted. The *I*–*V* curve in Figure 2b shows no threshold switching since the V_{th} of the neuron has exceeded 2.5 V, which means the neuron is inhibited. The current is only 5.9 µA at 2 V since the device is in NVHRS. To excite the neuron, a positive voltage sweeping is conducted (Figure 1e, red line). The current increases at 3.2 V, which means the HfO_2 is set to NVLRS. Applying the same stimulus (5 V, 200µs), the voltage oscillates between V_{th} and V_{hold}, as shown in Figure 2c. Figure 2d shows threshold switching as the voltage increases from 0 to 2.5 V, indicating HfO_2 is in NVLRS. The current reaches 100 µA (compliance current) at 2 V, indicating the adaptive neuron has high excitability.

To show the continuous adaptation of the neuron, the V_{th} is continuously tuned from 2.4 to 1.8 V by changing the conductance of HfO_2, as shown in Figure S4, Supporting Information. The correlation between V_{th} and conductance of HfO_2 (G_{HfO2}) can be expressed as

$$V_{th} = a * G_{HfO_2}^{b} \quad (1)$$

where $a = 0.35$ and $b = -0.198$. This adaptation behavior is of great significance for the research and application of artificial neurons.

Generally, the spiking frequency depends on the amplitude of the input stimuli within a certain range. In a proper range, the higher the input amplitude, the higher the spiking frequency. However, when the amplitude exceeds a certain level, the firing rates will decrease due to the internal protection mechanism of the neuron.[25] **Figure 3**a shows the dependence of spiking frequency on pulse amplitude. When the input pulse is above 4.5 V, the artificial adaptive neurons begin to oscillate. The oscillation frequency gradually increases with the pulse amplitude. However, the oscillation frequency decreases when the input

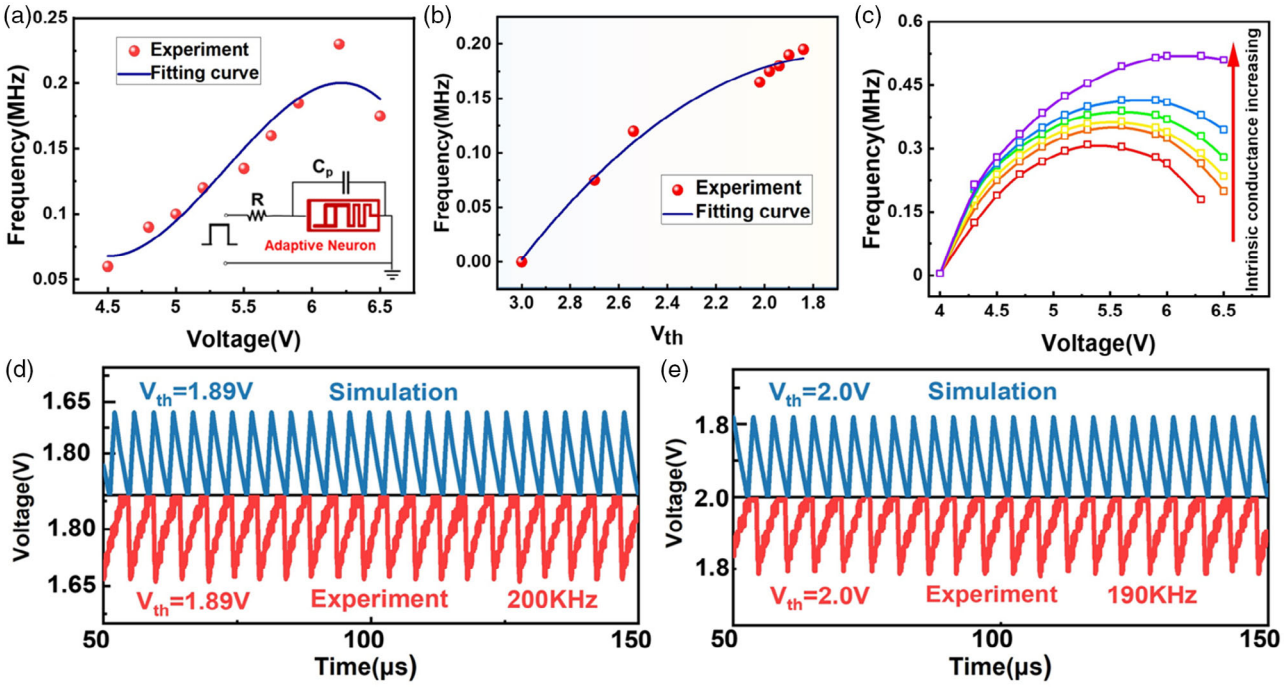

Figure 3. Intrinsic plasticity of the adaptive neuron. a) The correlation between input voltage and the firing frequency. The firing frequency first increases and then decreases with the increase of pulse amplitude. The blue is fitting curve. b) Dependence of spike firing rate on G_{HfO_2}. The spike firing rate of the adaptive neurons increases owing to the decrease of the V_{th} of the neuron. The blue is fitting curve. c) The simulation of firing frequency versus pulse amplitude and different G_{HfO_2}. In each conductance state, the correlation between the firing frequency and the pulse amplitude is similar: as pulse amplitude increases, the frequency first increases and then decreases. d–e) Comparison of measured neuron firing characteristics with simulated firing characteristics at Vth is 1.89 and 2 V, respectively. The oscillation frequency is 200KHz@ V_{th}=1.89 V, 190 KHz@ V_{th}=2.0 V. Red lines represent the experimental results and the blue lines is obtained through simulation.

is higher than 6.2 V. This is because the voltage is too large and the τ_{down} becomes longer. Eventually, the oscillation period is dominated by the discharge time. This mimics the protection mechanism of neurons to prevent neurons from aggressive stimulation.[26]

The intrinsic plasticity of neurons is experimentally demonstrated by setting the HfO_2 set to different conductance states. Under the same external resistance (230 KΩ) and input stimulus (5 V, 200 μs), the adaptive neuron achieved different responses. The spiking frequency increases from 40 to 200 KHz (Figure 3b). At $V_{th} = 1.89$ V and $V_{th} = 2$ V, the oscillation frequency is 200 and 190 KHz, respectively (Figure 3d,e, red line). The change of G_{HfO2} is equivalent to the change of intrinsic plasticity, which can emulate the adaptation of the biological neurons. In addition, a customized circuit model is established for further investigating the adaptive firing characteristics.[8] The simulation results (Figure 3d,e, blue line) are consistent with the experimental data. At each conductance state, the adaptive neuron shows similar spike firing characteristics: the frequency first increases as the increase of voltage and then decreases when voltage is beyond a certain range, as shown in Figure 3c.

4. Sequential Task Processing

Studies have shown that the intrinsic plasticity of neurons can store information related to previous experience[27] and exhibit a memory property.[28] The modulation of neuron threshold by changing G_{HfO_2} can be implemented to emulate the dependence on past experiences. An adaptive neuron will create a spiking pattern (during the presents of stimulus 1) when it is exclusively stimulated by a Poisson input stimulus 1 (red dots in **Figure 4**a). In contrast, if the neuron receives both stimulus 2 (blue dots in Figure 4a) and stimulus 1, meanwhile stimulus 2 is ahead of stimulus 1, a different spike firing pattern (during the presents of stimulus 1) will be evoked owing to its historical

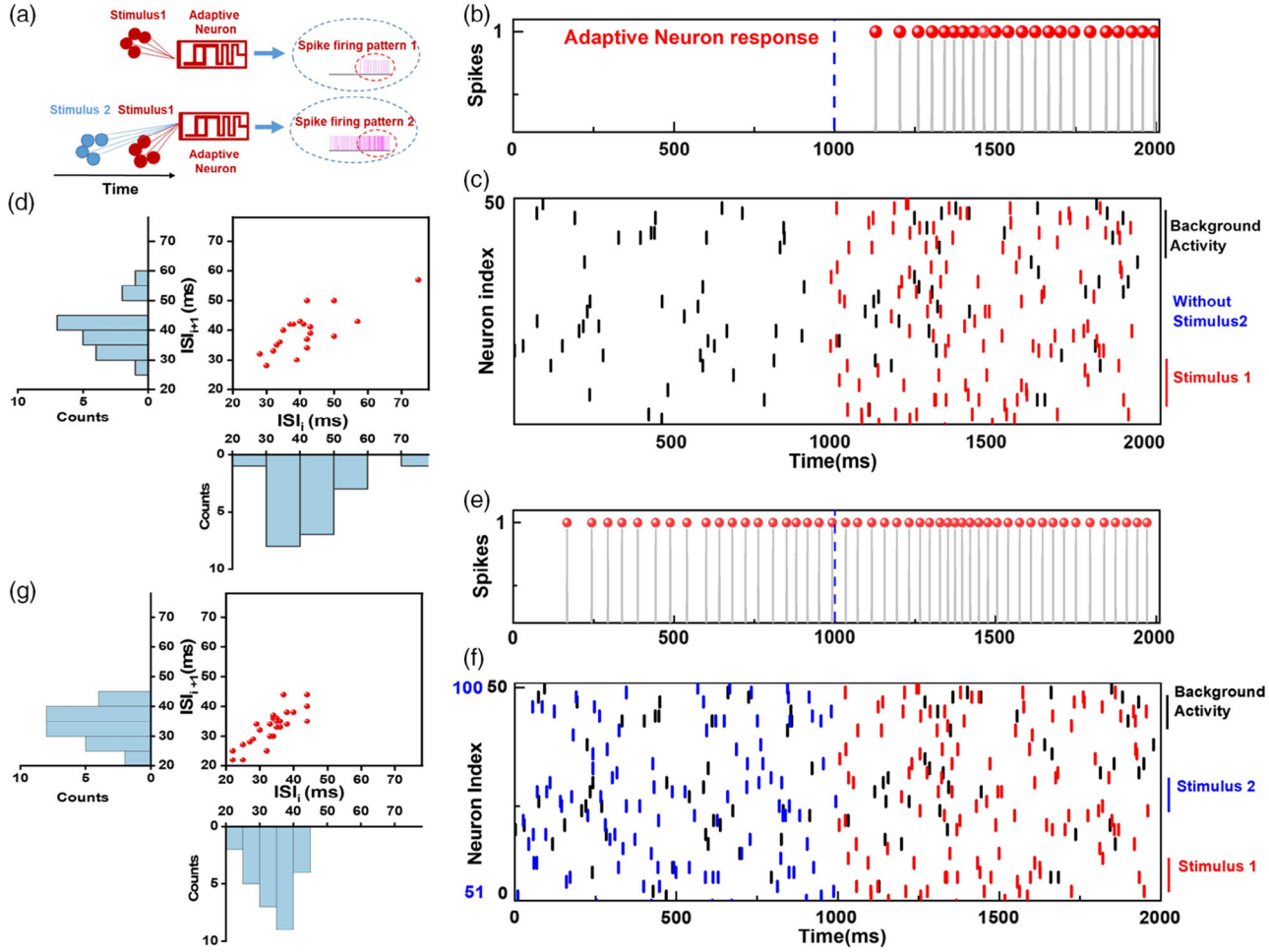

Figure 4. Illustration of the neuronal spiking-rate adaptation in processing serial order information. a) Schematic diagram of dependence of the adaptive neuron's response on historical input. b) The evoked responses to a sensory stimulus1 (red bars). c) The input spikes diagram of stimulus for (b) where only stimulus 1 is applied. The black bars represent the background noises (0.5 KHz Poisson input). After 1000 ms, the adaptive neuron receives stimulus 1 (1 KHz Poisson input) from 50 presynaptic neurons. d) The ISI distributions of the spikes when only receiving stimulus1. e) The evoked response to stimulus 2 (blue bars) and stimulus 1 (red bars) with specific order. f) The input spikes diagram of stimulus for (e) where two stimuli have specific order. The stimulus 2 arrives early (1000ms) than stimulus1. g) The ISI distributions of the spikes for receiving two ordered stimuli.

experience. A neuron model with an adaptive threshold voltage was built here for network simulations (details in the method section). The Na^+-conductance and K^+-conductance will influence the intrinsic plasticity of the biological neuron. When the Na^+-conductance is increased, more Na^+ will influx into the neuron in a short time, reducing the threshold of the neuron and causing a high firing rate.[29] In this demo, the G_{HfO2} is chosen to represent the Na^+-conductance. After a spike, the G_{HfO2} increases a small amount (ΔG_{HfO2}), and the V_{th} of the neuron decreases, which is equivalent to the effect of historical input. If G_{HfO2} exceeds a threshold conductance, it will be reset to the initial conductance owing to the internal protection mechanism of neurons. During the simulation (2000 ms), our adaptive neuron is subjected to a 0.5 KHz Poisson inputs stimulus (Figure 4c,f, black bars), which acts as background noises. After 1000 ms, the adaptive neuron is driven by a 1 KHz Poisson input from 50 presynaptic neurons (Figure 4c, red bars, stimulus1). The output spiking pattern (1000–2000 ms) is shown in Figure 4b. In contrast, if another stimulus2 (Figure 4f, blue bars) with the same input frequency is ahead of stimulus 1, the evoked firing pattern (1000–2000 ms) will be quite different, as shown in Figure 4e. After 1000 ms, the neuron produces a stronger response, generating an adapted firing pattern. This is because the G_{HfO_2} has been increased by stimulus2, lowering the V_{th} of the adaptive neuron.

By analyzing the spike patterns, the correlation pattern of the consecutive spike firings is obtained. Two inter-spike intervals (ISIs) are defined by the time difference between consecutive spikes (i.e., $\tau_n = t_n - t_{n-1}$, where t_n is the occurrence of the n_{th} spike). So the scatter plot of (t_n, t_{n+1}) pairs referred to as a return map can reveal the correlation between consecutive spikes. Figure 4d,g show the histograms of the ISIs distribution for the two response patterns within 1000–2000 ms, respectively. When only stimulus 1 is applied, the adaptive neuron exhibits irregular spiking, resulting in widely scattered (t_n, t_{n+1}) pairs. However, when stimulus2 and stimulus1 are applied in serial order, the neuron exhibits regular tonic spiking (t_n, t_{n+1}) pairs tightly clustered around a median value (33.46 ms).

Research have shown that this history-dependent manner is suitable for handling tasks that are sensitive to sequential inputs.[30] We demonstrated that the proposed adaptive neuron can deal with the computation tasks with a serial order of inputs,

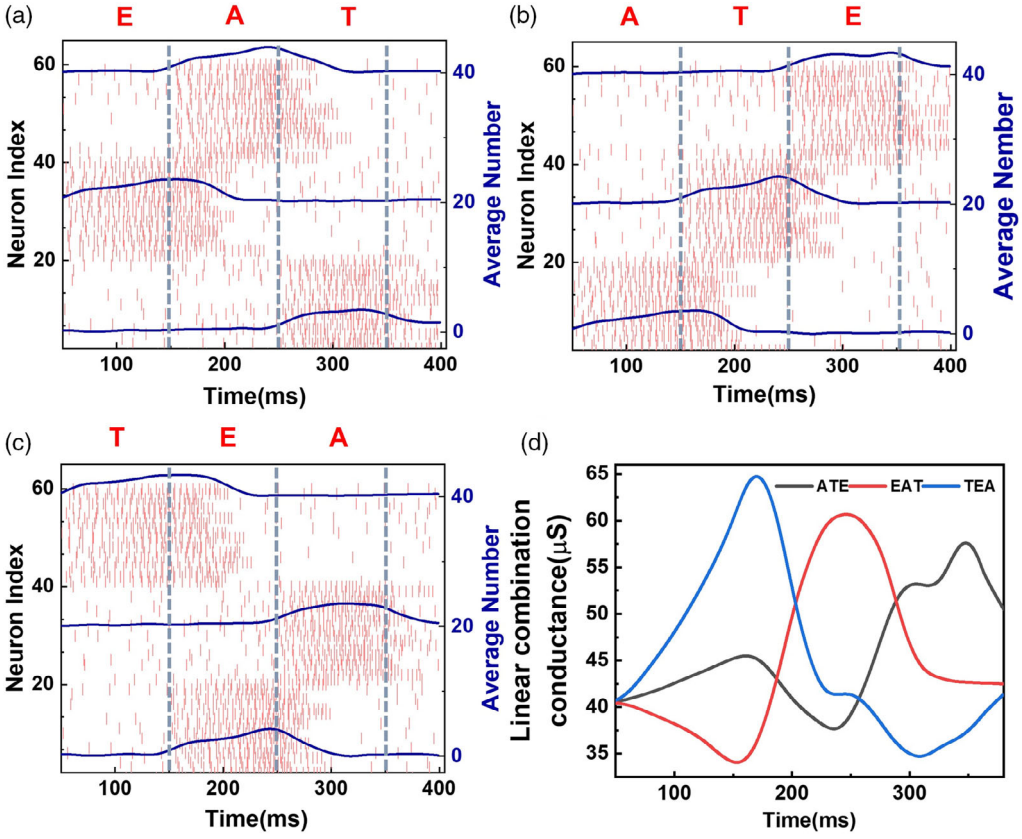

Figure 5. Neuron spiking-rate adaptation in processing word sequence recognition. "A," "E," and "T" are encoded as a same frequency Poisson input of the same frequency. a) Letters "E", "A," and "T" are randomly projected to 20 adaptive neurons. The duration of each stimulus is 100ms. The red line represents the evoked response. The blue line represents the average number of firing neurons in each subpopulation. b) Letters "A", "T," and "E" are randomly input to neurons as the same way. The evoked response (red line) and average number of firing neurons (blue line) are different from "E-A-T." c) Letters "T", "E," and "A" are randomly input to neurons as the same way. The evoked response (red line) and average number of firing neurons (blue line) are different from the previous two input orders. d) The linear combination average G_{HfO_2} traces during the entire simulation. It exhibits a memory characteristic. We can see that even if the stimulus is removed at 350 ms, the three G_{HfO_2} curves can still be distinguished.

such as word recognition. The meaning of a word is determined by the order of each letter. For example, swapping the order of letters "A," "E," and "T" can form three words "EAT," "ATE," and "TEA" with different meanings. To distinguish them, a population of adaptive neurons (60 neurons) is constructed. Each letter is encoded as a Poisson input with the same frequency. The three words are represented by sequences of three stimuli. Each stimulus is randomly projected to a subpopulation consisting of 20 adaptive neurons. Figure S5, Supporting Information, shows the Poisson stimuli input of the "TEA." The entire simulation time is 400 ms. The stimulus starts at $t = 50$ ms, and the duration of each stimulus is 100 ms. The evoked response of adaptive neurons for different stimuli is shown in **Figure 5**a–c (bars line). The blue line displays the average number of firing neurons in each subpopulation. It can be seen that even for the same letter input, the neuron group responds differently due to its historical memory. Figure 5d shows the linear combination average G_{HfO_2} traces during the entire simulation, exhibiting a memory characteristic clearly (details in the method section). It can be observed that the three G_{HfO_2} curves can still be distinguished even if the stimulus is removed at $t = 350$ ms. This phenomenon can be well explained by the memory effect of adaptive neurons. The information stored in the G_{HfO_2} can be subsequently retrieved by a linear readout.[31]

5. Conclusion

In summary, a novel adaptive neuron was designed and experimentally implemented with VO_2/HfO_2 dual-mode memristor. The neuronal excitability can be in materia modulated by continuously tuning the conductance of HfO_2, realizing the tunability of neuron intrinsic plasticity. This artificial adaptive neuron can switch between excitation and inhibition states. The intrinsic plasticity allows it to respond accordingly even to the same stimulus. A word recognition task involving letter sequences was demonstrated based on the proposed adaptive neuron. This work demonstrates the enrichment of neuron function is of great potential to empower the SNNs-based neuromorphic computing systems.

6. Experimental Section

Device Fabrication: The TiN/VO_2/HfO_2/Ti/Pt device was fabricated on n-Si wafers. First, 200 nm silicon oxide was deposited on Si substrate by low-pressure chemical vapor deposition (LPCVD) at 720 °C. Second, 50 nm Pt and 10 nm Ti were deposited by DC sputtering and patterned by the lift-off process as the bottom electrode (BE). Ti was used as an adhesion layer. Then, 5 nm HfO_2 and 30 nm VO_2 film were sequentially formed by atomic-layer deposition (ALD) and annealed in oxygen ambient at 450 °C for 30 min to crystallize VO_2. Finally, 20 nm TiN as the top electrode (TE) was formed by DC sputtering and patterned by the lift-off process.

Electrical Measurements: The DC sweep and pulse tests were carried out using the Agilent B1500A semiconductor parameter analyzer.

Neuron Model and Simulation: A leaky IF with variable threshold voltage was used in our simulations.[13] The threshold voltage V_{th} is related to G_{HfO_2}:$V_{th} = a * G_{HfO_2}^{b}$. The membrane voltage is described by the equation

$$C_m \frac{dV(t)}{dt} = \frac{-1}{R_m}(V(t) - V_{reset}) + I(t) - g_{ref}(t)(V(t) - E) \quad (2)$$

$$V(t) = \begin{cases} 1 & V(t) \geq Vth \\ V(t) & V(t) < Vth \end{cases} \quad (3)$$

where V_{reset} is the resting potential, R_m represents the leakage resistance, C_m is the membrane capacitance, and *I(t)* is the total input current at time t, and $g_{ref}(t)$ represents the effect of the refractory period. When the membrane potential reaches the threshold V_{th}, a spike occurs, and *V(t)* immediately returns to the V_{reset}. *E* represents the reversal potential. Following a spike, the G_{HfO_2} increased by ΔG_{HfO_2} and hence $V_{th} = a * (G_{HfO_2} + \Delta G_{HfO_2})^b$. If G_{HfO_2} exceeds the threshold conductance $G_{HfO_2\text{-th}}$, it will be reset to the initial conductance.

The conductance $g_{ref}(t)$ produces a period of relative inactivity. It decays exponentially with the time constant τ_1.

$$\frac{dg_{ref}(t)}{dt} = -\frac{g_{ref}(t)}{\tau_1} \quad (4)$$

During this simulation, the current I(t) was abruptly increased following the presynaptic spike, and then decays with a time constant τ_2.

$$I_{ij}(t) = I_{ij}(t-1) + w_{ij}\sum_{t_j}\delta(t - t_j) \quad (5)$$

$$\frac{dI_{ij}(t)}{dt} = -\frac{I_{ij}(t)}{\tau_2} \quad (6)$$

where w_{ij} is the synaptic weight between presynaptic neuron *j* and postsynaptic neuron *i*. $\delta()$ is the Dirac delta, and t_j are the spike times of presynaptic neurons. The total I(t) was the sum of the individual from the presynaptic neurons.

In Figure 5d, the conductance represents the linear readout of G_{HfO_2}.The linear combination of G_{HfO_2} ($LC\_G_{HfO_2}$) is calculated as follows

$$LC\_G_{HfO_2} = A * G_{1HfO_2} + B * G_{2HfO_2} + C * G_{3HfO_2} \quad (7)$$

where G_{1HfO_2}, G_{2HfO_2}, and G_{3HfO_2} represents the average conductance of neurons labeled 1–20, 21–40, and 41–60, respectively. *A*, *B*, and *C* are randomly generated random numbers between −1 and 1.

Acknowledgements

L.S. and Z.W. contributed equally to this work. This work was supported by the National Key Research and Development Project (No. 2019YFB2205401), the National Natural Science Foundation of China (No. 61834001, No. 62025401, No. 61904003, No. 61927901), in part by the "111" Project (No. B18001), in part by the Beijing Natural Science Foundation (No. 4212049), and in part by the PKU-Baidu Fund (No. 2020BD022).

Conflict of Interest

The authors declare no conflict of interest.

Data Availability Statement

The data that support the findings of this study are available from the corresponding author upon reasonable request.

Keywords

artificial adaptive neuron, intrinsic plasticity, neuromorphic computing systems, spike-rate adaptation

Received: December 16, 2021
Revised: February 14, 2022
Published online:

[1] A. Taherkhani, A. Belatreche, Y. Li, G. Cosma, L. P. Maguire, T. M. McGinnity, *Neural Networks* **2020**, *122*, 253.
[2] P. A. Merolla, J. V. Arthur, R. Alvarez-Icaza, A. S. Cassidy, J. Sawada, F. Akopyan, B. L. Jackson, N. Imam, C. Guo, Y. Nakamura, B. Brezzo, I. Vo, S. K. Esser, R. Appuswamy, B. Taba, A. Amir, M. D. Flickner, W. P. Risk, R. Manohar, D. S. Modha, *Science* **2014**, *345*, 668.
[3] N. Imam, T. A. Cleland, *Nat. Mach. Intell.* **2020**, *2*, 181.
[4] Z. R. Wang, S. Joshi, S. Savel'ev, W. H. Song, R. Midya, Y. N. Li, M. Y. Rao, P. Yan, S. Asapu, Y. Zhuo, H. Jiang, P. Lin, C. Li, J. H. Yoon, N. K. Upadhyay, J. M. Zhang, M. Hu, J. P. Strachan, M. Barnell, Q. Wu, H. Q. Wu, R. S. Williams, Q. F. Xia, J. J. Yang, *Nat. Electron.* **2018**, *1*, 137.
[5] Z. W. Wang, Q. L. Zheng, J. Kang, Z. Z. Yu, G. F. Zhong, Y. T. Ling, L. Bao, S. Y. Bao, G. D. Bai, S. Zheng, Y. M. Cai, J. Robertson, R. Huang, *IEEE Trans. Electron Devices* **2020**, *67*, 4166.
[6] Y. M. Cai, Z. W. Wang, Z. Z. Yu, Y. T. Ling, Q. Y. Chen, Y. F. Yang, S. Y. Bao, L. D. Wu, L. Bao, R. S. Wang, R. Huang, in *IEEE Inter. Electron Devices Meeting (IEDM)*, IEEE, San Francisco, CA, December **2020**.
[7] T. Tuma, A. Pantazi, M. Le Gallo, A. Sebastian, E. Eleftheriou, *Nat. Nanotechnol.* **2016**, *11*, 693.
[8] L. Bao, Z. W. Wang, B. W. Wang, K. Q. Liu, G. D. Bai, Z. Z. Yu, J. Kang, Y. T. Ling, L. D. Wu, Q. Y. Chen, K. M. Niang, Y. M. Cai, J. Robertson, R. Huang, *IEEE Electron Device Lett.* **2020**, *42*, 102.
[9] Y. C. Fang, Z. W. Wang, C. D. Cheng, Z. Z. Yu, T. Zhang, Y. C. Yang, Y. M. Cai, R. Huang, *Sci. China Inf. Sci.* **2019**, *62*, 1.
[10] X. M. Zhang, Z. H. Wu, J. K. Lu, J. S. Wei, J. Lu, J. X. Zhu, J. Qiu, R. Wang, K. H. Lou, Y. Z. Wang, T. Shi, C. M. Dou, D. S. Shang, Q. Liu, M. Liu, in *IEEE Inter. Electron Devices Meeting (IEDM)*, IEEE, San Francisco, CA, December **2020**.
[11] Z. Nadasdy, *Front. Syst. Neurosci.* **2009**, *3*, 6.
[12] J. Benda, *Curr. Biol.* **2021**, *31*, R110.
[13] H. Fitz, M. Uhlmann, D. Van den Broek, R. Duarte, P. Hagoort, K. M. Petersson, *Proc. Natl. Acad. Sci.* **2020**, *117*, 20881.
[14] H. K. Titley, N. Brunel, C. Hansel, *Neuron* **2017**, *95*, 19.
[15] G. Fuhrmann, H. Markram, M. Tsodyks, *J. Neurophysiol.* **2002**, *88*, 761.
[16] X. X. Wang, P. Huang, Z. Dong, Z. Zhou, Y. N. Jiang, R. Z. Han, L. F. Liu, X. Y. Liu, J. F. Kang, in *International Symposium on VLSI Technology, Systems and Application (VLSI-TSA)*, IEEE, Hsinchu, Taiwan, April **2018**.
[17] Y. Zhou, S. Ramanathan, *Proc. IEEE* **2015**, *103*, 1289.
[18] Z. H. Zhang, Z. W. Wang, T. Shi, C. Bi, F. Rao, Y. M. Cai, Q. Liu, H. Q. Wu, P. Zhou, *InfoMat* **2020**, *2*, 261.
[19] Z. W. Wang, J. Kang, G. D. Bai, G. F. Zhong, B. W. Wang, Y. T. Ling, Q. Y. Chen, L. Bao, L. D. Wu, Y. M. Cai, J. Robertson, R. Huang, *IEEE Electron Device Lett.* **2020**, *41*, 1009.
[20] S. Zhang, I. S. Kim, L. J. Lauhon, *Nano Lett.* **2011**, *11*, 1443.
[21] X. Wu, Y. Tao, L. Dong, Z. Wang, Z. Hu, *Mater. Res. Bull.* **2005**, *40*, 315.
[22] C. A. Campos, A. J. Bowen, S. Han, B. E. Wisse, R. D. Palmiter, M. W. Schwartz, *Nat. Neurosci.* **2017**, *20*, 934.
[23] D. Pimentel, J. M. Donlea, C. B. Talbot, S. M. Song, A. J. Thurston, G. Miesenböck, *Nature* **2016**, *536*, 333.
[24] O. Kiehn, *Nat. Rev. Neurosci.* **2016**, *17*, 224.
[25] R. A. Stetler, Y. Gao, A. P. Signore, G. Cao, J. Chen, *Curr. Mol. Med.* **2009**, *9*, 863.
[26] X. M. Zhang, Y. Zhuo, Q. Luo, Z. H. Wu, R. Midya, Z. R. Wang, W. H. Song, R. Wang, N. K. Upadhyay, Y. L. Fang, F. Kiani, M. Y. Rao, Y. Yang, Q. F. Xia, Q. Liu, M. Liu, J. J. Yang, *Nat. Commun.* **2020**, *11*, 1.
[27] C. Hansel, D. J. Linden, E. D'Angelo, *Nat. Neurosci.* **2001**, *4*, 467.
[28] J. T. Paz, S. Mahon, P. Tiret, S. Genet, B. Delord, S. Charpier, *J. Physiol.* **2009**, *587*, 3189.
[29] P. Dayan, L. F. Abbott, *Theoretical Neuroscience: Computational and Mathematical Modeling of Neural Systems*, Computational Neuroscience Series, MIT Press **2005**.
[30] R. Jackendoff, R. S. Jackendoff, *Foundations of Language: Brain, Meaning, Grammar, Evolution*, Oxford University Press **2002**.
[31] M. Rigotti, O. Barak, M. R. Warden, X. J. Wang, N. D. Daw, E. K. Miller, S. Fusi, *Nature* **2013**, *497*, 585.